Bulgarian Journal of Physics vol. **XX** (20XX) 1–10

Structural and Optical Characterization of Silver Sodium Niobate Perovskite Ceramics

Meenu Rani[1,2], **Y.P. Singh**[1], **Shilpi Jindal**[3*]

[1]Department of Physics Institute of Applied Sciences,
Mangalayatan University, Beswan, Aligarh, India
[2]Department of Physics, Hindu College Sonipat, India
[3]Department of Physics, Chandigarh University, Gharuan, Mohali, India
[*]Corresponding author E-mail: shilpi.85bansal@gmail.com

Received *19 September 2024*

Abstract. Lead-free polycrystalline sample of Silver Sodium Niobate (ANN) perovskite ceramics $Ag_{0.2}Na_{0.8}NbO_3$ had been synthesized by solid-state reaction approach for replacing lead-based ceramics. Structural and optical properties of prepared specimen had been investigated corresponding to room temperature. To find crystal structure, X-ray Diffraction (XRD) of powdered sample was done. Lattice parameters as well as the average crystallite size for specimen was determined using XRD data. XRD analysis revealed that synthesized sample of ANN had perovskite orthorhombic structure. Scanning Electron Microscopy (SEM) and the Energy Dispersive X-Ray Spectroscopy (EDX) were used to find microstructural properties. Average grain size of ANN sample was found to be 1.65 μm using ImageJ Software. Optical properties were studied with the help of Photoluminescence (PL) spectroscopy and Ultraviolet-Visible Diffuse Reflectance Spectroscopy (UV-VIS DRS).PL spectrum corresponding to excitation wavelength 400 nm had been recorded which showed the presence of visible emissions. Direct band gap was found to be 3.21 eV by Tauc plot. Fourier Transform Infrared (FTIR) spectrum of the sample showed a strong absorption peak at wavenumber 534 cm^{-1}. This was due to presence of Nb-O bond stretching and Nb-O-Nb bond bending.

KEY WORDS: ceramics, microstructural, optical, perovskite, photoluminescence, structural.

1 Introduction

A lot of attention is being drawn by ceramics possessing excellent physical as well as chemical properties over the last few years [1]. Ceramic materials having perovskite structure represented by the formula ABO_3 have been found as very good options in many applications on large scale owing to their superior

structural and physical properties [2–4]. In ABO_3, bigger cation A is generally monovalent, divalent or trivalent such as Ag^{+}, Na^{+}, Ca^{2+}, Ba^{2+}, La^{3+}, Bi^{3+} etc. belonging to alkaline or the rare earth family and smaller cation B is tetravalent or pentavalent belonging to transition metals such as Ti^{4+}, Nb^{5+}, etc. [5, 6]. Due to open nature of ABO_3 structure, there is a possibility of substitution by a number of different cations at A as well as B site that results in the extension of their physical and chemical properties such as ferroelectric, superconductivity, electrooptic, magnetoelectric, dielectric and piezoelectric properties. Perovskite materials are very important in many electronic applications for example-capacitors, electro-strictive actuators, detectors, transducers, sensors, memory devices etc. Generally, lead containing materials having superior ferroelectric, piezoelectric and pyroelectric properties are best for these applications, but due to toxic nature of lead, it leads to serious health and the environmental concerns. Therefore, it is essential to develop some suitable lead-free materials capable of replacing lead-bearing materials in all of these applications. Among these lead-free perovskite materials, silver niobate and sodium niobate are the perovskite oxides which have proved to be suitable alternative to lead containing compounds. Many researchers are putting efforts to investigate properties of these materials. Structural and the morphological properties of solid solution sodium lithium niobate $Li_{0.08}Na_{0.92}NbO_3$ had been studied and variation in electrical conductivity with temperature and frequency had been reported [7]. Sodium niobate ($NaNbO_3$) in powdered form using hydrothermal method had been prepared and characterized using X-ray Diffraction (XRD),Scanning Electron Microscopy (SEM),Atomic Force Microscopy (AFM), UV/VIS Spectroscopy and Fourier Transform Infrared Spectroscopy (FTIR) [8] Physical, dielectric and electrical properties of silver lithium niobate perovskite ceramics $Ag_{1-x}Li_xNbO_3$ ($x = 0, 0.3, 0.5, 0.7$) had been investigated [9]. In this work, sample of silver sodium niobate (ANN) $Ag_{0.2}Na_{0.8}NbO_3$ has been synthesized and its structural and optical studies have been done.

2 Experimental Details

Polycrystalline sample of Silver Sodium Niobate (ANN) with composition $Ag_{0.2}Na_{0.8}NbO_3$ had been prepared by solid-state reaction approach Highly pure (99.99%) silver oxide (Ag_2O), sodium carbonate (Na_2CO_3) and niobium pentoxide (Nb_2O_5) were used and weighed in correct stoichiometric ratio. After mixing and grinding, the sample was calcined for 2 hours at 1050°C in muffle furnace. Now, some drops of polyvinyl alcohol (PVA) were mixed in it and pellets of 10 mm diameter and 1 mm thickness was formed using hydraulic press. After that, sintering was done at 1150°C for 1 hour. For structural analysis, X-ray diffraction (XRD) was done on powdered sample on Phillips X-ray diffractometer using Cu K_α rays in 2θ range of 20° to 70°. Microstructure was analyzed on a Scanning Electron Microscope (SEM) (TESCAN VEGA

III LM) and Energy Dispersive X-Ray Spectrometer (EDX). To study photoluminescent properties, Photoluminescence (PL) spectrum of sample was taken with Fluorolog-3 (Horiba Jobin Yvon) spectrometer for excitation wavelength of 400 nm. Diffused reflectance spectrum of specimen had been recorded on Double beam UV/VIS /NIR Spectrophotometer, (Lambda 750, Perkin Elmer), USA. Perkin-Elmer Fourier Transform Infrared (FTIR) spectrometer was used to take infrared spectrum of specimen using KBr method.

3 Results and Discussion

3.1 Structural analysis

The recorded XRD pattern is displayed in Figure 1.

Corresponding to Bragg's angle $2\theta = 22.63°$, $22.83°$, $28.92°$, $32.07°$, $32.38°$, $41.55°$, $46.24°$, $46.68°$, $51.82°$, $52.34°$, $52.49°$, $57.39°$, $57.83°$ and $67.83°$, diffraction peaks are observed. These peaks correspond to (101), (020), (021), (200), (121), (131), (202), (040), (301), (103), (141), (321), (123) and (004) planes respectively. Joint Committee on Powder Diffraction Standards (JCPDS) data card No. 01-082-0606 ($NaNbO_3$) is utilized to index observed peaks [10]. Peak with maximum intensity is seen at 32.38? corresponding to (121) plane. Diffraction peaks noted at 22.83?, 32.07?, 67.83? have been taken to determine interplanar spacing and unit cell parameters a, b and c. The calculated data

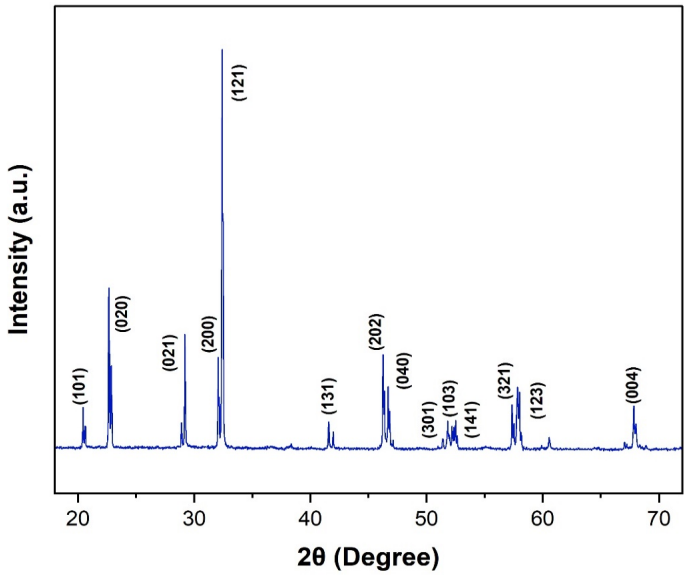

Figure 1. XRD pattern of $Ag_{0.2}Na_{0.8}NbO_3$.

confirms that specimen has perovskite orthorhombic structure. Similar crystal structure for niobates has been previously reported [7,9]. Tolerance factor (t), is found using equation (1) that determines stability of phase.

$$t = \frac{0.2r_{\text{Ag}} + 0.8r_{\text{Na}} + r_{\text{O}}}{\sqrt{2}(r_{\text{Nb}} + r_{\text{O}})}\,, \tag{1}$$

where r_{Ag} is the ionic radius of Ag^{+} (1.15 Å), r_{Na} is the ionic radius of Na^{+} (1.02 Å), r_{Nb} is the ionic radius of Nb^{5+} (0.64 Å) (all CN = 6) and r_{O} is the ionic radius of O^{2-} (1.40 Å). The value of t as calculated came out to be 0.848. As the value of t lies between 0.71 and 0.9 that indicates the synthesis of stable orthorhombic perovskite sample. To calculate average crystallite size, D of specimen Scherrer's formula given in equation (2) has been used [11]

$$D = \frac{K\lambda}{\beta\cos\theta}\,. \tag{2}$$

In this equation, K shows Bragg's constant whose value is 0.94, λ shows wavelength of the CuK_{α} rays with value 1.54056 Å, β shows the full width at half maxima and θ shows Bragg's angle for diffraction peak with maximum intensity in XRD pattern. Equation (3) is used to calculate lattice microstrain

$$\varepsilon = \frac{\beta}{4\tan\theta}\,. \tag{3}$$

Volume of unit cell is determined by equation (4) [12]

$$V = a \times b \times c\,. \tag{4}$$

To determine X-ray density, equation (5) is used [13]

$$\rho_{\text{X-ray}} = \frac{Z\,M_w}{N_{\text{A}}V}\,, \tag{5}$$

where Z, M_w, N_{A} and V respectively are number of atoms in one unit cell, the molecular mass of sample, Avogadro's number and volume of unit cell. Equation (6) [14] has been used to calculate the bulk density

$$\rho_{\text{bulk}} = \frac{m}{v}\,, \tag{6}$$

where m and v are mass and volume of the pellet formed. Using values of $\rho_{\text{X-ray}}$ and ρ_{bulk}, %Porosity is found with the help of equation (7) [15]

$$\%\text{Porosity} = \left(1 - \frac{\rho_{\text{bulk}}}{\rho_{\text{X-ray}}}\right) \times 100\,. \tag{7}$$

All calculated crystallographic parameters are shown in Table 1.

Table 1. Crystallographic parameters of $Ag_{0.2}Na_{0.8}NbO_3$

Crystal structure	Orthorhombic	Average crystallite size D [nm]	63.03
Lattice parameters:		Lattice microstrain ε	2.06×10^{-3}
a [Å]	5.5182	Tolerance factor t	0.848
b [Å]	7.8410	$\rho_{\text{X-ray}}$ [g/cm^3]	6.289
c [Å]	5.5178	ρ_{bulk} [g/cm^3]	5.095
Unit cell volume V [Å^3]	238.75	%Porosity	18.99

3.2 Microstructural analysis

Obtained SEM micrograph of sample is displayed in Figure 2(a). It is clear that the grains of varying size are found in sample. To obtain average grain size, image J software is used and average grain size came out to be 1.65 μm. To show distribution of grain size, histogram is plotted as revealed in Figure 2(b). To study elemental composition, Energy Dispersive X-ray Spectroscopy (EDX) of sample has been performed and the recorded spectrum is shown in Figure 2(c). Prominent peaks for required elements Ag, Na, Nb and O have been noted in EDX spectrum.

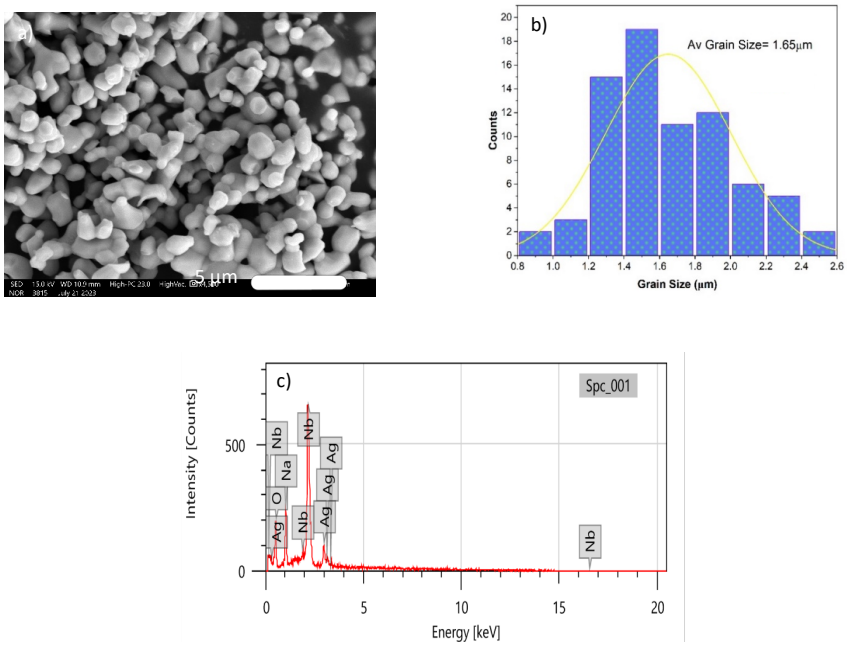

Figure 2. (a) SEM image; (b) Histogram plot; (c) EDX spectrum of $Ag_{0.2}Na_{0.8}NbO_3$.

3.3 Photoluminescence analysis

Photoluminescence (PL) spectrum of synthesized specimen was taken corresponding to excitation wavelength of 400 mm and is shown in Figure 3.

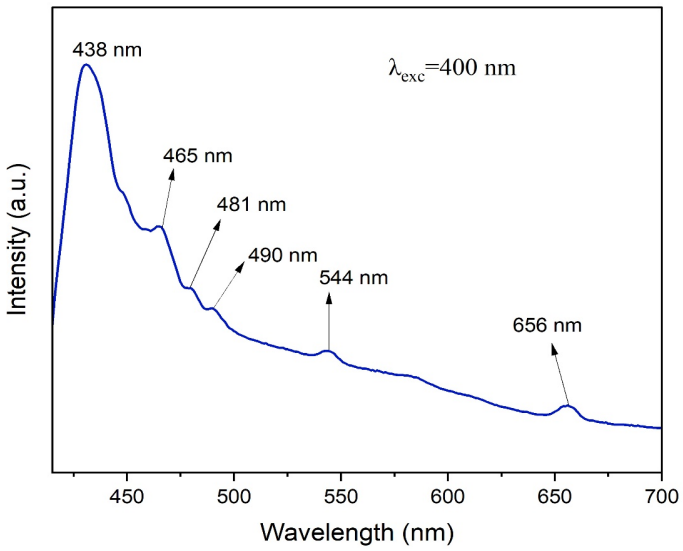

Figure 3. PL spectrum of $Ag_{0.2}Na_{0.8}NbO_3$.

Emission peaks corresponding to the wavelengths 438 nm, 465 nm, 481 nm, 490 nm, 544 nm and 656 nm have been observed. For calculating the energy band gap E_g in eV for this wavelength equation (8) has been used

$$E_g\ [\text{eV}] = \frac{1240}{\lambda\ [\text{nm}]}\,. \tag{8}$$

The corresponding band gaps as calculated are 2.83 eV, 2.67 eV, 2.58 eV, 2.53 eV, 2.28 eV and 1.89 eV respectively. Peaks at 438nm,465nm, 481nm and 490 nm are attributed to blue emission band and at 544 nm and 656 nm to green and red emission bands respectively. Observed blue emission band is due to $[NbO_6]^{7-}$ luminescent group present in niobate materials [16]. Existence of oxygen vacancies in specimen leads to emission of green band. These visible emissions indicate the suitability of prepared specimen in laser generation in visible range, optoelectronic devices like LED's and telecommunication devices.

3.4 DRS analysis

For determination of band gap for direct allowed transitions, Diffuse Reflectance Spectroscopy (DRS) had been performed on powdered specimen. In order to

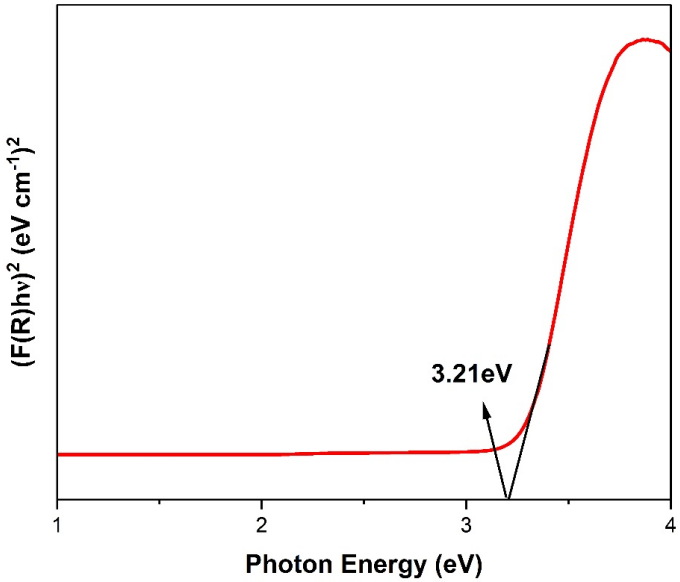

Figure 4. Tauc plot of $Ag_{0.2}Na_{0.8}NbO_3$.

calculate band gap of specimen, use of Kubelka-Munk theory had been done [17, 18]. Kubelka-Munk function $F(R)$ is given in equation (9) [19, 20]

$$F(R) = \frac{1 - R^2}{2R}\,. \tag{9}$$

Recorded reflectance has been converted into absorption using $F(R)$ and Tauc plot has been drawn as shown in Figure 4.

In this plot, energy $h\nu$ of incident photon is taken along X-axis and the modified Kubelka-Munk function $[F(R)h\nu]^2$ is taken along Y-axis. Then a tangent to linear region of curve is drawn and extrapolated to meet X-axis at a point. Value of energy corresponding to this point provides the direct band gap of specimen and it comes out to be 3.21 eV.

3.5 FTIR analysis

Recorded Fourier transform infrared spectrum over wavenumber range 4000 cm^{-1} to 400 cm^{-1} is depicted in Figure 5.

In the spectrum, a strong absorption peak at wavenumber 531 cm^{-1} is observed which can be related to Nb-O stretching and the Nb-O-Nb bond bending [8]. Multiple peaks at 1421 cm^{-1}, 1462 cm^{-1}, 1569 cm^{-1} and 1695 cm^{-1} have also been observed. They are related to presence of Na-O vibrations [21]. Nb-O bond length is calculated corresponding to absorption peak observed at 531 cm^{-1} with

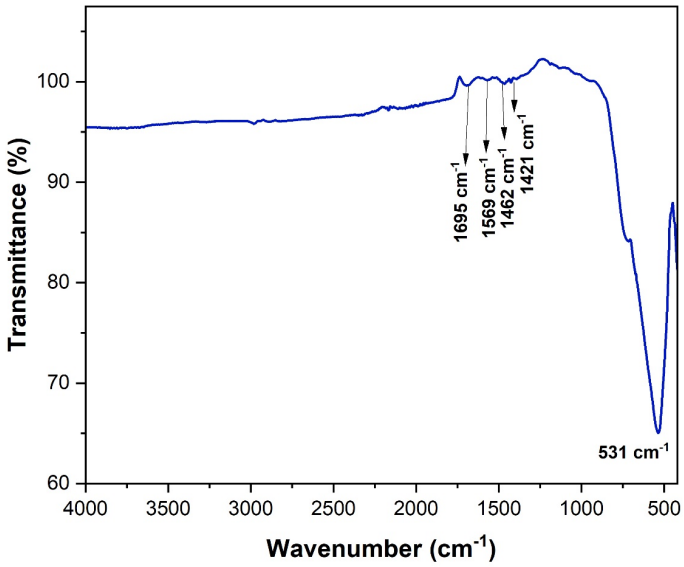

Figure 5. FTIR spectrum of $Ag_{0.2}Na_{0.8}NbO_3$.

the help of Badger's rule. The formula used to determine bond length; R is given in equation (10) [22, 23]

$$R = \sqrt[3]{\frac{c_{ij}}{K}} + d_{ij}\,. \tag{10}$$

Here K represents force constant in Mdynes/cm, and c_{ij} and d_{ij} are fitting constants and their values for Nb-O bond are 0.490 Å and 1.18 Å respectively [23]. For calculation of force constant K, Hooke's law is employed and equation (11) is used [24]

$$v = \frac{1}{2\pi c}\sqrt{\frac{K}{\mu}}\,. \tag{11}$$

In above equation, μ is the reduced mass of Nb and O atoms. Force constant K as calculated comes out to be 0.22677338 Mdynes/cm and Nb-O bond length came out to be 2.47280 Å.

4 Conclusion

A polycrystalline sample of silver sodium niobate having composition $Ag_{0.2}Na_{0.8}NbO_3$ has been synthesized through solid state reaction. Stable perovskite orthorhombic structure was confirmed for the sample by XRD analysis. SEM micrograph indicated the presence of grains of varying size with average grain size 1.65 μm. Photoluminescent spectrum depicted the presence of visible

emission bands revealing the use of sample in production of laser in the visible range and in different optoelectronic and telecommunication devices. Tauc plot determined direct band gap of sample to be 3.21 eV. A strong absorption peak at wavenumber 531 cm^{-1} has been observed in FT-IR spectrum corresponding to stretching of Nb-O bond and bending of Nb-O-Nb bond.

Bibliography

[1] E.R. Camargo, F.L. Souza, E.R. Leite, M. Kakihana (2004) Structural and electrical characterization of dense lead zirconate titanate ceramics synthesized by the oxidant-peroxo wet-chemical route. *J. Appl. Phys.* **96**(4) 2169-2172.

[2] A.K. Tomar, A. Joshi, G. Singh, R.K. Sharma (2021) Perovskite oxides as supercapacitive electrode: Properties, design and recent advances. *Coord. Chem. Rev.* **431** 213680.

[3] A. Anantharaman, T.L. Ajeesha, J. Baby, M. George (2020) Effect of structural, electrical and magnetooptical properties of CeMnxFe1-xO3-δ perovskite materials. *Solid State Sci.* **99** 105846.

[4] D. Zhang, X. Zhang, X. Li, Z. Liang, H. Xu, Z. Lv, X. Sang, S. Li (2021) Effect of BaO–CaO–SiO2 addition on dielectric and electrocaloric properties of lead-free 0.2Ba(Ti0.9Sn0.1)O3-0.8Ba(Zr0.18Ti0.82)O3 bulk ceramics. *Solid State Sci.* **119** 106684.

[5] F. El Bachraoui, Y. Tamraoui, S. Louihi, J. Alami, R. Shahbazian-Yassar, Y. Yuan, K. Amine, B. Manoun (2021) Unusual superparamagnetic behavior in bulk Ba0.198La0. 784Ti0.096Fe0.8O3δ. *Mater. Res. Bull.* **137** 111187.

[6] F. El Bachraoui, Z. Chchiyai, Y. Tamraoui, H. El Moussaoui, J. Alami, B. Manoun (2022) Optical and magnetic properties of perovskite materials: Ba0.3La0.7Ti0.3Fe0.7O3 and Ba0.1La0.9Ti0.1Fe0.9O3. *J. Rare Earth.* **40**(4) 652-659.

[7] W. Śmiga, B. Garbarz-Glos, M. Livinsh, A. Kalvane (2011) Structural and Electric Properties of Sodium Lithium Niobate Ceramic Solid Solution Li0.08Na0.92NbO3. *Ferroelectrics* **418**(1) 88-93.

[8] P. Vlazan, P. Sfirloaga, F. Stefania Rus (2016) Dedicated to Professor Mircea Diudea on the Occasion of His 65th Anniversary Synthesis and characterization of lead free sodium niobate powder. **Vol.1.**

[9] O.P. Nautiyal, S.C. Bhatt (2013) Physical and Dielectric Properties of Silver Lithium Niobate Mixed Ceramic System. *Am. J. Mater. Sci. Eng.* **1**(3) 54-59.

[10] JCPDS Data Card Number 01-082-0606.

[11] M. Aadil, S. Zulfiqar, M.F. Warsi, P.O. Agboola, I. Shakir (2020) Free-standing urchin-like nanoarchitectures of Co3O4 for advanced energy storage applications. *J. Mater. Res. Technol.* **9**(6) 12697-12706.

[12] M.H. Carvalho, E.C. Pereira, A.J.A. De Oliveira (2018) Orthorhombic SnO2 phase observed composite (Sn1-xCex)O2 synthesized by sol-gel route. *RSC Adv.* **8**(8) 3958-3963.

[13] S.A. Salman, F.I. Hussain, N.A. Bakr (2016) Structural study of Ba1-xCaxTiO3 ceramic perovskite material using X-ray diffraction analysis. *J. Nano Adv. Mater*. **4**(1).

[14] M. Aadil, S. Zulfiqar, H. Sabeeh, M.F. Warsi, M. Shahid, I.A. Alsafari, I. Shakir (2020) Enhanced electrochemical energy storage properties of carbon coated Co3O4 nanoparticles-reduced graphene oxide ternary nano-hybrids. *Ceram. Int.* **46**(11) 17836-17845.

[15] A. ur Rehman, M. Aadil, S. Zulfiqar, P.O. Agboola, I. Shakir, M.F.A. Aboud, S. Haider, M.F. Warsi (2021) Fabrication of binary metal doped CuO nanocatalyst and their application for the industrial effluents treatment. *Ceram. Int.* **47**(5) 5929-5937.

[16] G. Blasse, M.G.J. Van Leur (1985) Luminescence and energy transfer in the columbite structure. *Mater. Rres. Bull.* **20**(9) 1037-1045.

[17] C. Aydın, O.A. Al-Hartomy, A.A. Al-Ghamdi, F. Al-Hazmi, I.S. Yahia, F. El-Tantawy, F. Yakuphanoglu (2012) Controlling of crystal size and optical band gap of CdO nanopowder semiconductors by low and high Fe contents. *J. Electroceram.* **29** 155-162.

[18] T.V. Vineeshkumar, D.R. Raj, S. Prasanth, N.V. Unnikrishnan, V.M. Pillai, C. Sudarasanakumar (2018) Fe induced optical limiting properties of Zn1-xFexS nanospheres. *Optics Laser Technol.* **99** 220-229.

[19] R. Maity, A.P. Sakhya, A. Dutta, T.P. Sinha (2019) Investigation of concentration dependent electrical and photocatalytic properties of Mn doped SmFeO3. *Mater. Chem. Phys.* **223** 78-87.

[20] A. El Hachmi, B. Manoun, M. Sajieddine, Y. Tamraoui, S. El Ouahbi (2021) Synthesis, structural and optical properties of perovskites-type: Sr3Fe2+xMo1-xO9-3x/2 (x = 0.30, 0.45, 0.60, 0.75 and 1.00). *Polyhedron*. **200** 115133.

[21] S.K. Roy, S.N. Singh, K. Kumar, K. Prasad (2013) Structural, FTIR and ac conductivity studies of NaMeO3 (Me = Nb, Ta) ceramics. *Adv. Mater. Res.* **2**(3) 173.

[22] M. Kaupp, D. Danovich, S. Shaik (2017) Chemistry is about energy and its changes: A critique of bond-length/bond-strength correlations. *Coord. Chem. Rev.* **344** 355-362.

[23] R.M. Badger (1935) The relation between the internuclear distances and force constants of molecules and its application to polyatomic molecules. *J. Chem. Phys.* **3**(11) 710-714.

[24] S. Kaya, E. Chamorro, D. Petrov, C. Kaya (2017) New insights from the relation between lattice energy and bond stretching force constant in simple ionic compounds. *Polyhedron* **123** 411-418.